NMR Physics: Measuring T_1 and T_2 of Diluted Glycerin

Francisca Vasconcelos*
MIT Department of Physics
(Dated: November 27, 2019)

In this work, pulsed nuclear magnetic resonance (NMR) is used to measure characteristic material properties. In particular, the $\boldsymbol{T_1}$ and $\boldsymbol{T_2}$ decay times are estimated for varying concentrations of glycerin and water. This is achieved using the *Three-Pulse Sequence* and the *Carr-Purcell Pulse Sequence*, respectively. Each of these quantities provides a better understanding of how different relaxation processes, such as rethermalization and decoherence, vary in these different mixtures.

I. INTRODUCTION

Nuclear Magnetic Resonance, or NMR, was first used independently by Felix Bloch [1] and Edward Purcell [2], in the late 1940s, to measure nuclear magnetic moments. Since then, the technology has progressed significantly, serving as the basis for MRI health-imaging technology [3] and as a platform for quantum computation [4, 5]. Generally speaking, such measurements provide interesting information about the microscopic structure of a system of magnetic dipoles, through macroscopic perturbations. This work explores different relaxation processes which can occur in these spin ensembles.

II. THEORY

II.1. Nuclear Magnetism

Quantum mechanics governs that particles (such as electrons, protons, and nuclei) have an intrinsic quantized angular momentum, known as *spin*. For spin-$\frac{1}{2}$ particles, there are two possible configurations: "spin-up" (value $+\frac{\hbar}{2}$) and "spin-down" (value $-\frac{\hbar}{2}$). Thus, the wavefunction of this spin system can be described by a complex superposition of the spin-up and spin-down eigenstates. Such a two-level system can be visualized as a vector lying in a two-dimensional, complex Hilbert space known as the *Bloch sphere*. For further discussion of the Bloch sphere representation, refer to *Appendix A*.

If a charged particle is placed in a magnetic field, it will undergo a quantum precession, analogous to Larmor precession. For more information about classical Larmor precession and the resulting free induction, refer to *Appendix B*. While there are several key differences between this quantum precession of a single magnetic moment and classical Larmor precession, the *expectation* of the quantum magnetic moment indeed behaves like the classical magnetic moment (in the limit of a large number of repeated measurements, as dictated by Ehrenfest's Theorem). Rather than performing repeated measurements of a single quantum spin, NMR makes use of an *ensemble* measurement of a large number of spins simultaneously.

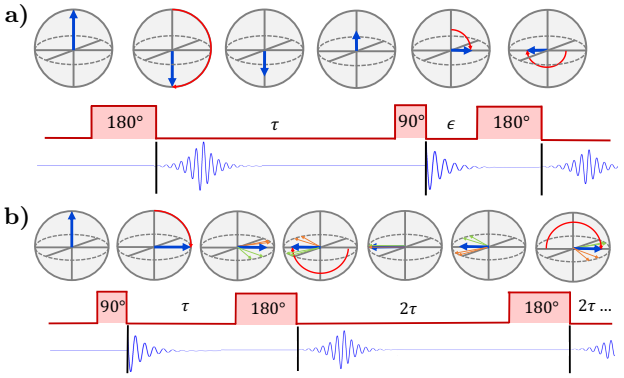

FIG. 1. NMR pulse sequences used to measure relaxation processes. Applied pulses are illustrated in red, while the spin ensemble response is in blue (for the Bloch sphere and free induction NMR signal). **(a)** The *Three-Pulse Sequence* is used to measure *Spin-Lattice Relaxation*, characterized by the $\boldsymbol{T_1}$ time. **(b)** The *Carr-Purcell Pulse Sequence* is used to measure *Spin-Spin Relaxation*, characterized by the $\boldsymbol{T_2}$ time.

If these spins are *coherent*, then the ensemble should act like a macroscopic, classical magnetic moment.

II.1.1. Pulsed NMR

It is necessary to manipulate the state of the spin ensemble to study different relaxation processes. The solenoid used to read transverse magnetization can also be used to generate an RF field around the sample. If the applied RF magnetic field freuency is on resonance with the Larmor frequency of the sample, the state vector precesses about the $\hat{x}$-axis of the Bloch sphere. This rate of precession is much slower than the Larmor frequency.

By varying the time the RF field is applied to the sample, we can force the state vector to move to different points of interest on the Bloch sphere. For this experiment, $\frac{\pi}{2}$ and π rotations about the $\hat{x}$-axis, known as the 90° pulse and the 180° pulse respectively, were necessary for the pulse sequences described in the next section.

II.2. Relaxation Mechanisms

Due to the macroscopic nature of nuclear magnetization, any measurable free induction will not last long. Individual perturbed spins return to equilibrium through a

* francisc@mit.edu

process known as *relaxation*, reducing the observable free induction signal. For illustrations of these relaxation processes, refer to *Appendix C*.

II.2.1. Spin-Lattice Relaxation

The spin-lattice relaxation process describes the longitudinal motion of the spin ensemble magnetization towards the ground state, due to *rethermalization*. This is called "spin-lattice" relaxation because individual spins dissipate energy to the surrounding lattice environment, causing relaxation to the lowest energy configuration. In this experiment, an *inversion recovery* procedure is used to measure the characteristic time constant governing this decay process, denoted $\boldsymbol{T_1}$.

II.2.2. Spin-Spin Relaxation

The second relaxation process of interest describes randomization in the precessional motion of individual spins, due to interactions with the magnetic fields of neighboring spins. This causes spins which were originally precessing in-phase with the ensemble to *decohere*. They thus destructively interfere with the ensemble magnetization, reducing the observed transverse magnetization. The characteristic time constant governing this decay process is denoted $\boldsymbol{T_2}$.

III. EXPERIMENTAL SETUP

III.1. Glycerin Samples

In order to observe how $\boldsymbol{T_1}$ and $\boldsymbol{T_2}$ change as a function of relative glycerin-water concentration, seven different samples were used: Glycerin-98%, Glycerin-93%, Glycerin-70±0.16%, Glycerin-50±0.06%, Glycerin-20±0.07%, Tap Water (Glycerin-0%), and Deionized Water (Glycerin-0%).

III.2. Measurement Chain

The measurement chain for the MIT Junior Lab NMR setup is quite complex, so we provide a high-level overview, as illustrated in Fig. 2. For the full specification, refer to the JLAB manual [6].

The central control system for the experiment is the NMR probe. This combines signals (via a phase detector) from the RF pulse generator and magnet (with a magnetic field of roughly $1.7T$) for measurement on the oscilloscope. It also contains a digital pulse programmer, used to specify the parameters and frequency of RF pulses sent to the magnet. The *Three-Pulse* and *Carr-Purcell* pulse sequences are pre-programmed into the controller, but users can specify coarse timing for two independent pulse widths, a wait time between pulses (τ), and the temporal spacing between pulse sequences. Determination of the Larmor frequency of the sample and the pulse width for the 90°/180° pulse, as described in *Appendix D* and *Appendix E*, is necessary for this experiment.

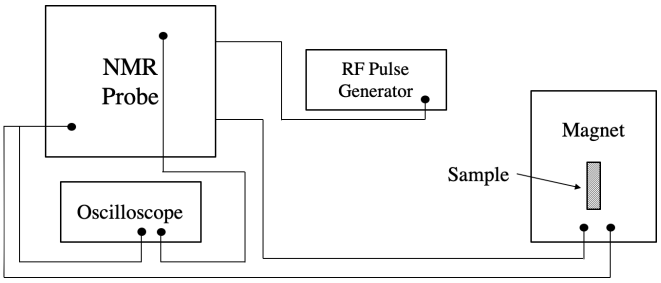

FIG. 2. The experimental measurement chain consists of an RF pulse generator connected to an NMR probe to control the magnet which encompass the glycerin sample. An oscilloscope is used to readout pulse and measurement signals.[a]

[a] Figure by Ghadah Alshalan

III.3. Three-Pulse Sequence to Measure T_1

In order to measure decay due to spin-lattice relaxation, the *Three-Pulse Sequence* was used. As illustrated in Fig. 1, this sequence consists of a 180° pulse followed by a delay of time τ, a 90° pulse, a very small delay of time ϵ, and a final 180° pulse.

The initial 180° pulse rotates the spin ensemble to the excited, or $|1\rangle$, state. During the wait time, τ, spins will randomly rotate towards the ground, or $|0\rangle$, state. On average, the ensemble will decohere along the z-axis of the Bloch sphere, through the origin and towards the $|0\rangle$ state. However, since there is no transversal component, the magnetization amplitude of the ensemble cannot be determined. Thus, a 90° pulse is used to rotate the ensemble onto the transverse plane, generating a readable transverse maganetization which can be used to determine how much the state decohered. Finally, a 180° pulse is applied almost instantaneously, flipping the orientation of the spin ensemble in the transverse plane and generating a spin-echo.

The max amplitude of the spin-echo is the desired quantity for measurement, since it corresponds to the magnetization amplitude of the spin ensemble. In the experiment, for each value of τ, the NMR free induction signal was displayed on an oscilloscope and the amplitude of the spin-echo was measured/recorded. In order to determine $\boldsymbol{T_1}$, these recorded values (M_z) were fit temporally to the curve,

$$M_z(\tau) = |M_0(1-2)e^{-\frac{\tau}{\boldsymbol{T_1}}}| \tag{1}$$

For further discussion as to why this curve is expected theoretically, refer to *Appendix F*. Note, however, that the final 180° pulse of the *Three-Pulse Sequence* is not necessary, but used because it is easier to read the max amplitude of a spin-echo than that of a 90° FID-decay.

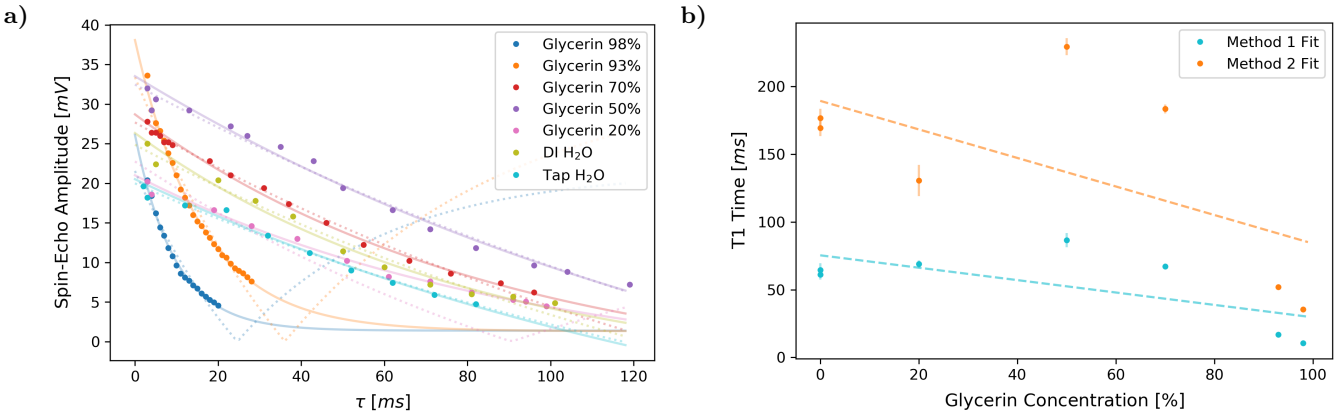

FIG. 3. **(a)** Measurements of spin-echo amplitude for increasing τ values in the *Three-Pulse Sequence*. Two different fits were performed, according to Eqn 1 (dashed line, Method 1) and Eqn 3 (solid line, Method 2). **(b)** For each fit method, the predicted $\boldsymbol{T_1}$ times were plotted and used to perform a linear fit.

In fact, $\boldsymbol{T_1}$ can be inferred from measurement of the peak of the FID after the 90° pulse instead.

III.4. Carr-Purcell Pulse Sequence to Measure $\boldsymbol{T_2}$

In order to measure decay due to spin-spin relaxation, the *Carr-Purcell Pulse Sequence* was used. As illustrated in Fig. 1, this sequence consists of a 90° pulse followed by a delay of time τ, a 180° pulse, a delay of time 2τ, another 180° pulse, another delay of time 2τ, and so forth.

The initial 90° pulse rotates the spin ensemble onto the $\hat{x}$-axis of the transverse plane. During the wait time, τ, individual spins interact with neighboring spins and magnetic fields, deviating from the ensemble precession. On average, the ensemble decoheres along the $\hat{x}$-axis, towards the origin of the Bloch sphere. However, the 180° pulse causes the spins to flip orientation, but continue precessing as before during the ensuing 2τ delay time. Since the delay is double the initial τ delay, the spins realign briefly along the $\hat{x}$-axis before decohering again, generating a spin-echo. The peak amplitude of this spin-echo is proportional to the magnetization of the decohered spin ensemble after time τ. By repeatedly using a 2τ wait time, the previous decoherence is measured and the state decoheres more before the next measurement.

In order to determine $\boldsymbol{T_2}$, the peak amplitude of all the spin-echoes (M_xy) are fit temporally to the curve

$$M_xy(t) = M_0 e^{-\frac{t}{\boldsymbol{T_2}}} \tag{2}$$

IV. DATA ANALYSIS

IV.1. $\boldsymbol{T_1}$ Time Estimation

Experimentally, we did not observe the expected resurgence in the spin-echo amplitudes. For theory on why this is expected, refer to *Appendix F*. Additionally, given limited device access, data was only recorded for $\tau < \boldsymbol{T_1}\ln(2)$, i.e. before the inflection point of Eqn 1.

For each sample, the recorded spin-echo amplitudes were fit to Eqn. 1, with M_0 and $\boldsymbol{T_1}$ as free parameters. The uncertainty in the predicted $\boldsymbol{T_1}$ was found using the square-root of the magnitude of the corresponding diagonal entry of the fit covariance matrix. The χ^2 and χ^2_r of the fit were also calculated. However, it was noted that the theoretically predicted curve did not seem to fit the data well. Thus, the same procedure was performed again, fitting to an exponential decay with offset,

$$M_z(\tau) = M_0 + (M - M_0)e^{-\frac{\tau}{\boldsymbol{T_1}}}, \tag{3}$$

where M, M_0, and $\boldsymbol{T_1}$ were free parameters. The results from both methods are reported in *Appendix G*.

While there was no theoretical model, we anticipated a linear relationship in $\boldsymbol{T_1}$ relative to glycerin-concentration. However, as can be seen by the fits to both methods in Fig 3, the data did not fit particularly well to this model. Method 1 (2) predicted a slope of -0.458±0.228 (-1.053±0.609) and offset of 75.37±13.93 (189.38±37.14), with $\chi^2 = 79.46$ (179.49), $df = 6$ (6), and $\chi^2_r = 13.2$ (29.74).

IV.2. $\boldsymbol{T_2}$ Time Estimation

Depending on the number of spin-echo amplitudes used in the fit to Eqn. 2, a drastically different $\boldsymbol{T_2}$ could be predicted. We attempted to address this using two different fitting methods. In the first fit method, only the first three spin-echo amplitudes were used, avoiding the resurgence/plateau seen in later spin-echo amplitudes.

In the second fit method, these resurgence values were instead considered. Since there is a theoretical form for the decay, $n-1$ independent fits were performed, where n is the total number of spin-echos from the Carr-Purcell measurement. For the first fit, only the first two spin-echo amplitudes were used. For each of the following $n-2$ fits, the number of fit points was incremented by one. For every fit, the predicted M_0 and $\boldsymbol{T_2}$ values as well as the χ^2 and χ^2_r were recorded. The three-parameter and

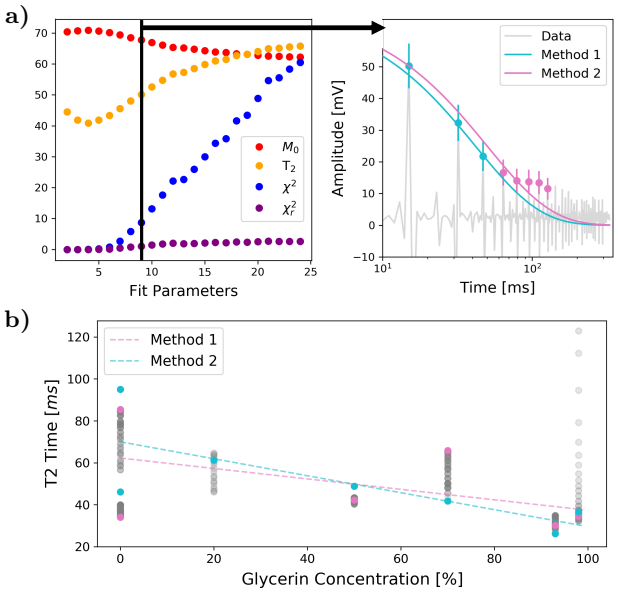

FIG. 4. **(a)** Method 2 determined an "optimal" number of spin-echo amplitudes to use in the Eqn 2 fit. **(b)** The predicted $\boldsymbol{T_2}$ times for all numbers of parameters are plotted in grey, with opacity inversely proportional to their χ^2_r. $\boldsymbol{T_2}$ for the first three parameters (Method 1) and for the "optimal" number of parameters (Method 2) are highlighted, respectively, in blue and pink. A linear fit was performed for the results of each method.

"optimal"-parameter values can be found in *Appendix H*. As illustrated in Fig 4 for the Glycerin-70% sample, these values do, in fact, change depending on the number of parameters used in the fit. To determine the "best" fit, we used the number of parameters which minimized $|\chi^2_r - 1|$. For the Glycerin-70% sample, this was nine fit parameters. Fig 4 compares the nine-parameter fit of this method to the three-parameter fit of the first method. For plots of all samples, refer to *Appendix I*.

The outcomes of all the fits for each sample concentration is plotted in grey in Fig 4, with opacity inversely proportional to χ^2_r. The predicted values from the first and second fit method are, respectively, colored in pink and blue. Linear fits were performed for the output of each of these fit methods. Method 1 (2) predicted a slope of -0.249±0.193 (-0.404±0.157) and an offset of 62.268±11.572 (70.003 ± 9.554), with χ^2 =40.752 (21.475), $df = 6$, and χ^2_r =6.792 (3.579).

V. RESULTS & CONCLUSIONS

Since no resurgence was observed, we believe there was a critical error in the T_1 measurement procedure. Quantitatively, this was reinforced by the improved fit of the exponential fit of Eqn 3 (with large positive offset), relative to the true resurgence-based fit of Eqn 1. It is hard to say what caused this error, given the difficulties with the apparatus and limited time to run the experiment. Provided more time, we would re-perform the entire experiment, collecting data for larger τ, verifying the pulse widths, and performing repeated measurements. However, with the data we were able to collect, it seems that T_1 should decrease with increased glycerin-concentration. Furthermore, the decrease in T_1 for low glycerin concentration (relative to the Glycerin-50% sample) could be explained by the relatively low viscosity of water, allowing increased particle/spin mobility within the sample and potential for interactions.

The $\boldsymbol{T_2}$ measurements were affected by both statistical and systematic uncertainty. The signal fluctuated slightly temporally, which was addressed by recording and averaging five independent measurements of the NMR free induction spin-echo sequence from the oscilloscope. However, there still remained a significant noise floor. During experimentation it was noted that by wiggling loose components, the noise floor could be significantly affected. In future experiments this could be eliminated by ensuring all components are secure. Overall, the most significant source of uncertainty was the resurgence of the spin echo after dropping to a near-zero quantity. We believe that this can be attributed to miscalibration of the pulse width or an insufficient delay time between spin-echos, but further tests would be required to verify these theories. Ultimately, however, with a unique fitting procedure, we dealt with this uncertainty qualitatively and showed a roughly linear trend in $\boldsymbol{T_2}$ time relative to glycerin concentration.

Overall, we demonstrated that $\boldsymbol{T_1}$ and $\boldsymbol{T_2}$ vary as a function of glycerin concentration. Given time to take more precise measurements, these predicted quantities and trends could be used to identify unknown samples and infer their properties.

ACKNOWLEDGMENTS

FV gratefully acknowledges Ghadah Alshalan's equal partnership, as well as the guidance and advice of the JLAB course staff and faculty.

[1] F. Bloch, Phys. Rev. **70**, 460 (1946).
[2] N. Bloembergen, E. M. Purcell, and R. V. Pound, Phys. Rev. **73**, 679 (1948).
[3] P. T. Callaghan, *Principles of nuclear magnetic resonance microscopy* (Oxford University Press on Demand, 1993).
[4] D. G. Cory, A. F. Fahmy, and T. F. Havel, Proceedings of the National Academy of Sciences **94**, 1634 (1997).
[5] I. L. Chuang, N. Gershenfeld, M. G. Kubinec, and D. W. Leung, Proceedings of the Royal Society of London. Series A: Mathematical, Physical and Engineering Sciences **454**, 447 (1998).
[6] *JLAB NMR Manual* (MIT Physics Department).

Appendix A: Bloch Sphere Representation of Spins

A two-level quantum system has two eigenstates: spin-up, $|0\rangle$, and spin-down, $|1\rangle$. These eigenstates serve as a basis for all possible system states, which can be represented as

$$|\Psi\rangle = u|0\rangle + d|1\rangle, \tag{A1}$$

where $|u|^2 + |d|^2 = 1$. This system is governed by the Schrödinger Equation,

$$i\hbar\frac{d}{dt}|\Psi\rangle = H|\Psi\rangle, \tag{A2}$$

with NMR Hamiltonian,

$$H = -\boldsymbol{\mu}\cdot\boldsymbol{B} = -\mu(\sigma_x B_x + \sigma_y B_y + \sigma_z B_z), \tag{A3}$$

where σ_x, σ_y, and σ_z are Pauli matrices.

The two-level system lies in a two-dimensional, complex Hilbert space, known as the *Bloch sphere* and shown in Fig 5. Thus, a system in the state $u|0\rangle + d|1\rangle$ can be represented as a vector pointing in the direction (θ, ϕ), where $u = cos(\theta/2)$ and $d = e^{i\phi}sin(\theta/2)$. It is not possible to detect a global phase of the system. Thus, the so-called Bloch vector has coordinates $(\cos\phi\sin\theta, \sin\phi\sin\theta, \cos\theta)$.

Note that this is a rotating reference frame, in the case of NMR precessing at the Larmor frequency. Furthermore, we can represent the effect of NMR pulses on the Bloch vector as rotation matrices. For example, rotation about the $\hat{x}$-axis is governed by,

$$R_x(\beta) = e^{-i\beta\sigma_x/2} = \cos\left(\frac{\beta}{2}\right)\mathbb{I} - i\sin\left(\frac{\beta}{2}\right)\sigma_x. \tag{A4}$$

Finally, as illustrated in Fig 5, measurement in our NMR apparatus occurs about the $\hat{x}$-axis.

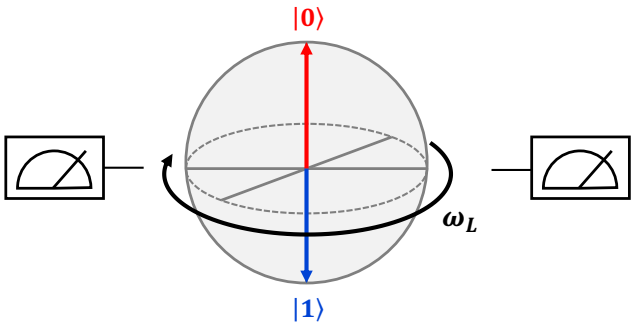

FIG. 5. The Bloch sphere representation of our NMR quantum system.

Appendix B: Larmor Precession & Free Induction

In classical electromagnetism, a charged body with non-zero angular momentum, $\boldsymbol{L}$, has a magnetic moment, $\boldsymbol{\mu}$, related to its intrinsic gyromagnetic ratio, γ, as

$$\boldsymbol{\mu} = \gamma\boldsymbol{L}. \tag{B1}$$

The gyromagnetic ratio is constant and depends on the mass and charge distribution of the body. When placed in a static magnetic field, $\boldsymbol{B_0}$, the magnetic moment experiences a torque,

$$\frac{d\boldsymbol{L}}{dt} = \boldsymbol{\mu}\times\boldsymbol{B_0}, \tag{B2}$$

where $\boldsymbol{L}$ is the axis of rotation.

In the case of a spherical body of mass with uniform charge distribution ($\gamma_{cl} = \frac{q}{2m}$), we observe a phenomenon known as *Larmor precession*. Regardless of the angle, α, between $\boldsymbol{L}$ and $\boldsymbol{B_0}$, the body precesses at the rate

$$\boldsymbol{\omega_L} = -\gamma_{cl}\boldsymbol{B_0}, \tag{B3}$$

where $\omega_L = |\boldsymbol{\omega_L}|$ is the *Larmor frequency*. This precession is applicable to our NMR system, as illustrated in Fig 6.

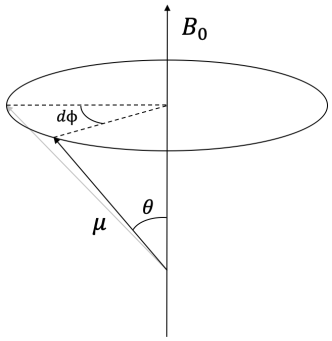

FIG. 6. The magnetic moment $\boldsymbol{\mu}$ precesses about the magnetic field $\boldsymbol{B_0}$, at angle θ, in this semi-classical view of NMR.[a]

[a] Figure by Ghadah Alshalan

If $\boldsymbol{B_0} = B_0\hat{\boldsymbol{z}}$, we define the x-y plane as the *transverse plane*. Imagine we place a solenoid around the magnetic moment, along the $\hat{x}$ direction in the transverse plane, and α is nonzero. In this case, a component of $\boldsymbol{\mu}$ lies in the transverse plane, generating an oscillatory magnetic field at frequency ω_L and inducing a measurable emf of

$$V(t) = V_0(\alpha)cos(\omega_L t + \phi_0), \tag{B4}$$

where ϕ_0 depends on the angle between $\boldsymbol{\mu}$ and the solenoid. It is important to note that $V_0 = 0$ when $\alpha = 0, \pi$ and has maximum amplitude when $\alpha = \pm\frac{\pi}{2}$. The detected voltage $V(t)$ is known as the *free induction NMR* signal and is used to understand the bulk material properties of a sample. The measured free induction decay (FID) following the application of a 90° pulse is illustrated in Fig 7.

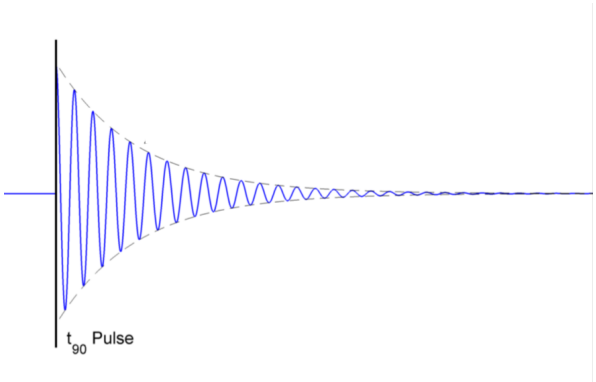

FIG. 7. After applying a 90° pulse to our NMR system, we will observe a free induction decay envelope as shown in grey. The carrier frequency, in blue, results from the mixing of the Larmor frequency and input function-generator frequency.[a]

[a] Figure from JLAB Manual [6]

Appendix C: Relaxation Mechanisms (Illustrated)

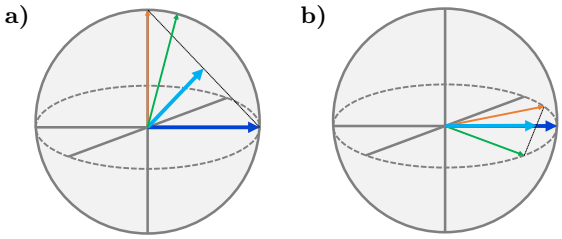

FIG. 8. After applying a 90° pulse, relaxation processes deteriorate the ensemble spin magnetization (colored in blue) through random interactions of individual spins (colored in orange and green) with the environment and other spins. Note that, for simplicity, we only show deviations of two spins. In the actual setup, the ensemble consists of thousands of individual spins. **(a)** In *Spin-Lattice Relaxation* spins lose energy to the environment and decay to the ground, or $|0\rangle$, state. **(b)** In *Spin-Spin Relaxation* spins interact with the magnetic fields of neighboring dipoles and precess faster/slower than the Larmor frequency of the ensemble.

Appendix D: Finding the Larmor Frequency

The NMR probe used in our experiment delivers RF power to the magnet surrounding the sample. Using the function generator, we can control the frequency, ω, of the signal sent to magnet. The signal returned to the oscilloscope is the mixture of this signal with the FID emitted by the sample, at the Larmor frequency $\omega_L = \gamma B_0$. This mixed signal has a beat frequency consisting of a high-frequency, $|\omega + \omega_L|$, and a low-frequency, $|\omega - \omega_L|$ component. While the high-frequency component exceeds the measurement capability of the oscilloscope, the low-frequency component serves as the carrier frequency of our measured signal (with the FID envelope), as illustrated in Fig 7.

In order to find the Larmor frequency, it is simply necessary to modify the frequency of the function generator until $|\omega - \omega_L| = 0$. This value of ω can be observed on the oscilloscope, when the carrier frequency disappears and only the FID envelope is visible. For the purposes of our experiment, however, we were not interested in the exact determination of the Larmor frequency. The carrier-frequency is actually beneficial to observing the spin-echos for determination of $\boldsymbol{T_1}$ and $\boldsymbol{T_2}$. However, in order to ensure interaction with the sample, it was necessary that ω not be too far off resonance with ω_L. Since the Larmor frequency of most of the glycerin samples was fairly constant, $\omega = 7.512$MHz was used for all of the experiments.

Appendix E: Finding Pulse Widths

In order to determine the 90° and 180° pulse widths, it is solely necessary to find the 180° pulse width and divide the time by two for 90°. The 180° pulse width is easier to find because, assuming our system is initialized in the $\rangle$ state, the 180° pulse should flip the spin ensemble to the $\rangle$ state. In theory, both the $|0\rangle$ and $|1\rangle$ states are perpendicular to the transverse plane, meaning that the observable transverse magnetization should be zero. Thus, we can start our pulse width at the minimum time of $\tau = 1$ and continuously increment it until we see that the magnetization is minimized.

Given the coarse control provided by the NMR probe (we can only increment τ by multiples of 1ms), it is unlikely that we will find the exact 180° pulse width (meaning the 90° pulse will also be off), which is a limitation of our experimental setup and source of systematic uncertainty. This miscalibration would cause us to under- or over-rotate our spin-ensemble, creating interesting artiacts in the $\boldsymbol{T_1}$ and $\boldsymbol{T_2}$ measurements.

Appendix F: Three-Pulse Sequence Theory

The *Three-Pulse Sequence* involves repeated measurement of the decoherence of the $|1\rangle$ state, for increasing wait times, τ. After applying the 180° pulse, if τ is small, the state will not have much of a chance to decohere before the 90° and 180° pulses are applied for measurement along the transverse plane. This means that the measured magnetization will be large and oriented in the negative direction. However, as τ is increased, the state will decohere more, moving closer to the origin, before measurement. This will cause the measured transverse magnetization to remain negative, but to decrease in magnitude. However, for even large τ times, the state will decay past the origin and flip orientation, generating a positive transverse magnetization. As *tau* increases further, the state progresses closer to $|0$, increasing the measured magnetization. Eventually the spin ensemble will reach the $|0$ state and the measured transverse mag-

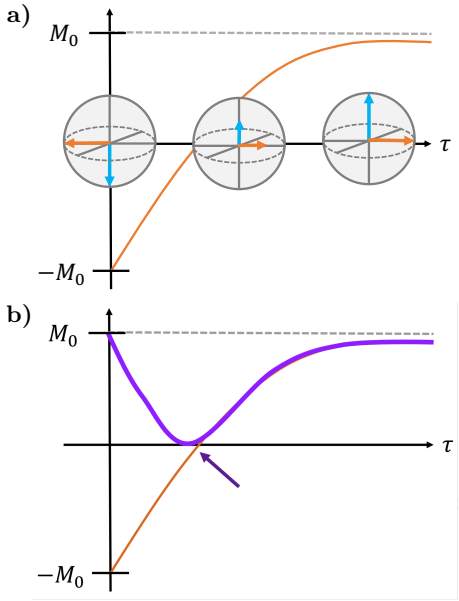

FIG. 9. **(a)** The expected magnetization measurement curve of the *Three-Pulse Sequence*. The Bloch spheres demonstrate the state of the spin-ensemble after the first 180° pulse and decay of time τ (blue), as well as the state after the following application of the 90°/180° pulses for measurement. **(b)** In practice, we can only measure the absolute value of the transverse magnetization. The inflection point of the *Three-Pulse Sequence* measurement curve occurs at $\tau = \boldsymbol{T_1}\ln(2)$.

netization will saturate at the max value. This process is illustrated in Fig 9.

With our experimental apparatus, it is extremely difficult to distinguish positive from negative orientation directly from the FID signal, due in part to the Larmor precession. Thus, we only measure the absolute value of the magnetization, resulting in Eqn 1. Due to the form of this curve, we expect to observe an inflection point/minima at $\tau = \boldsymbol{T_1}\ln(2)$. The expected curve and inflection point is illustrated in Fig 9.

Appendix G: T_1 Fit Data

TABLE I. $\boldsymbol{T_1}$ fit data for Method 1 (fit to resurgence curve).

Sample	98%	93%	70%	50%	20%	DI	Tap
$\boldsymbol{T_1}$	10.63	16.83	67.25	86.60	68.95	61.21	64.63
$\Delta\boldsymbol{T_1}$	0.28	0.26	1.95	5.17	2.80	3.80	5.03
χ^2	0.444	0.319	0.437	1.736	0.366	0.909	0.805
df	17	25	16	14	11	10	9
χ^2_r	0.026	0.013	0.027	0.124	0.033	0.091	0.089

TABLE II. $\boldsymbol{T_1}$ fit data for Method 2 (fit to offset exponential).

Sample	98%	93%	70%	50%	20%	DI	Tap
$\boldsymbol{T_1}$	9.56	15.80	86.41	165.81	94.60	82.22	164.60
$\Delta\boldsymbol{T_1}$	0.39	0.60	8.87	47.81	15.018	17.61	87.41
χ^2	0.196	0.214	0.235	0.841	0.195	0.766	0.288
df	17	25	16	14	11	10	9
χ^2_r	0.012	0.009	0.015	0.060	0.018	0.766	0.032

Appendix H: T_2 Fit Data

TABLE III. $\boldsymbol{T_2}$ fit data for Method 1 (first 3 spin-echoes). Note that $df = 2$ for all these measurements.

Sample	98%	93%	70%	50%	20%	DI	Tap
$\boldsymbol{T_2}$	41.84	26.26	36.68	48.89	61.30	46.15	95.06
$\Delta\boldsymbol{T_2}$	1.81	1.27	11.30	16.21	9.06	6.79	3.02
χ^2	0.026	0.044	1.309	0.868	0.064	0.092	0.001
χ^2_r	0.013	0.022	0.654	0.434	0.032	0.046	0.000

TABLE IV. $\boldsymbol{T_2}$ fit data for Method 2 ("optimal" spin-echoes).

Sample	98%	93%	70%	50%	20%	DI	Tap
# Params	9	8	6	9	3	6	25
$\boldsymbol{T_2}$	50.14	30.19	34.40	42.30	61.30	34.11	85.39
$\Delta\boldsymbol{T_2}$	4.79	3.38	5.07	4.47	9.06	5.42	10.10
χ^2	8.738	7.670	5.416	8.352	0.064	5.148	21.425
df	8	7	5	8	2	5	24
χ^2_r	1.090	1.096	1.083	1.044	0.032	1.030	0.893

Appendix I: T_2 Fit Plots

1. Glycerin-98%

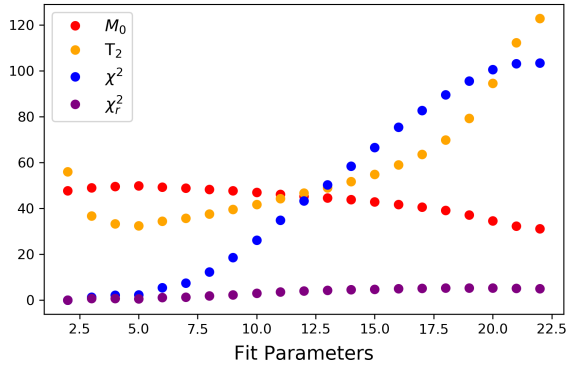

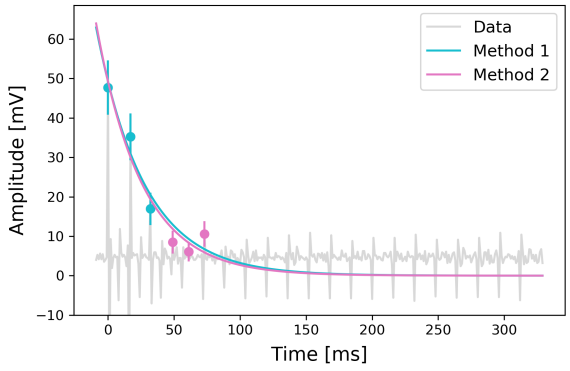

2. Glycerin-93%

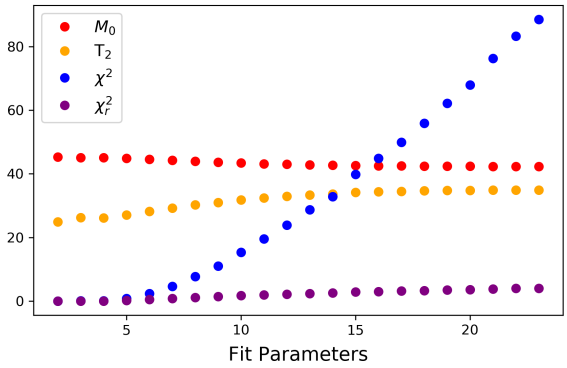

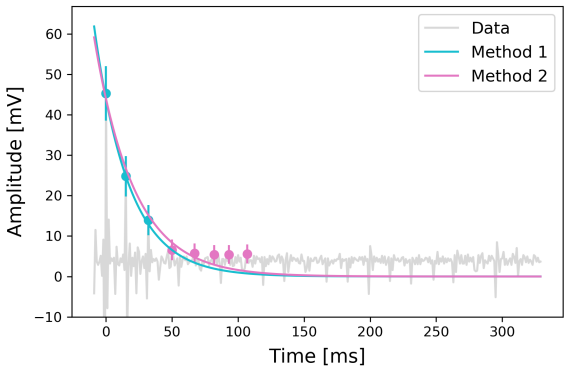

4. Glycerin-50%

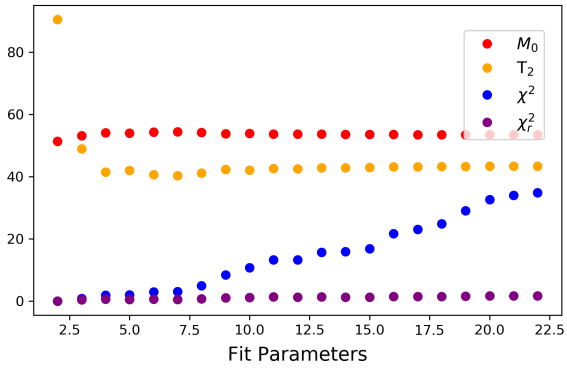

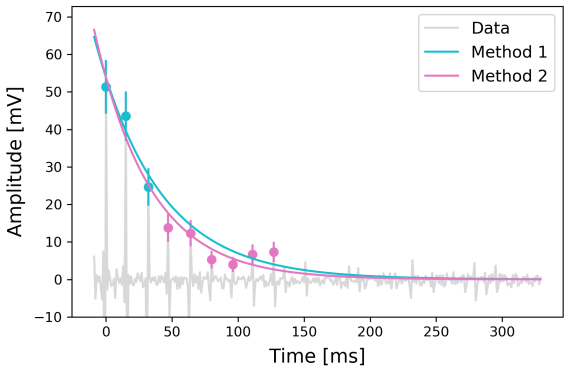

3. Glycerin-70%

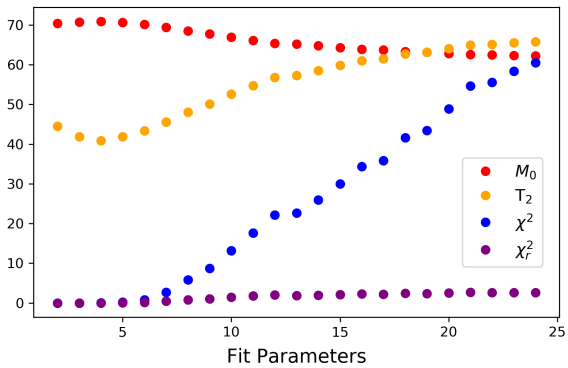

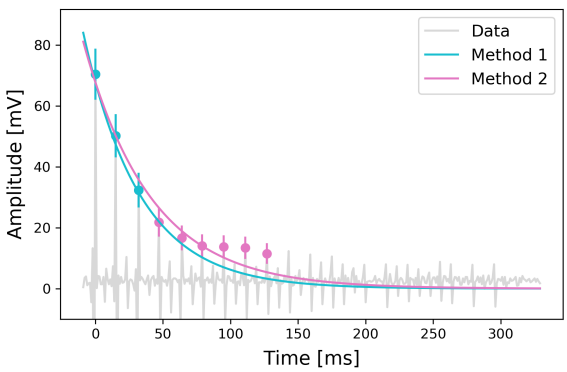

5. Glycerin-20%

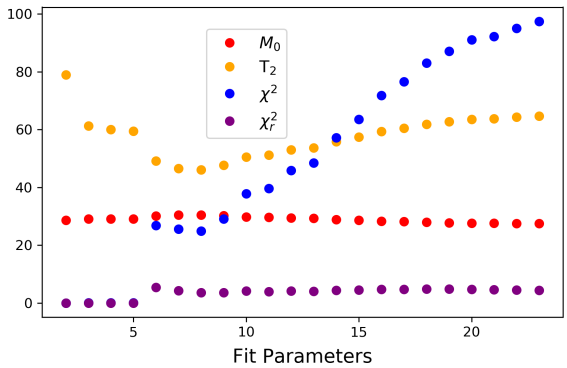

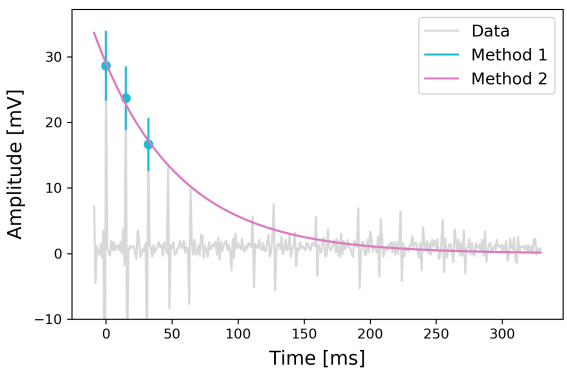

6. Distilled H_2O

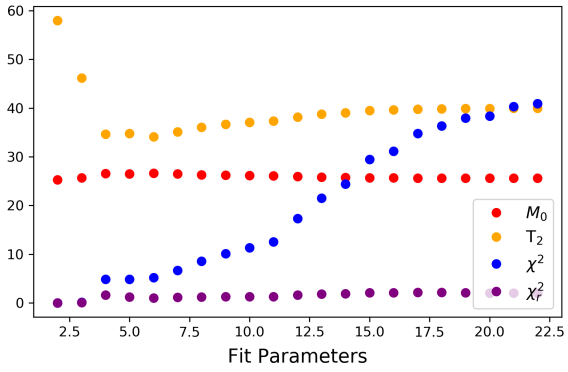

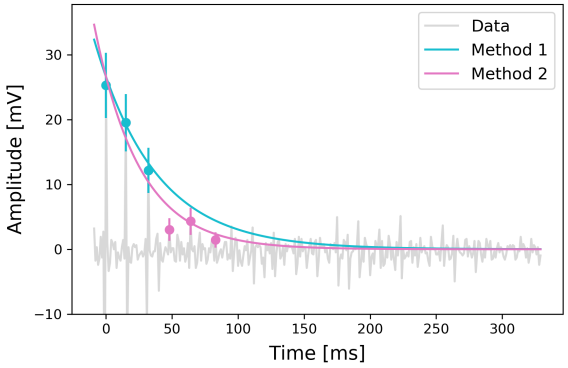

7. Tap H_2O